Chemico-Biological Interactions 309 (2019) 108714

Contents lists available at ScienceDirect

Chemico-Biological Interactions

journal homepage: www.elsevier.com/locate/chembioint

The *in vitro* protective effects of the three novel nanomolar reversible inhibitors of human cholinesterases against irreversible inhibition by organophosphorous chemical warfare agents

Maja D. Vitorović-Todorović[a,*], Franz Worek[b], Andrej Perdih[c], Sonja Đ. Bauk[a], Tamara B. Vujatović[d], Ilija N. Cvijetić[c,e]

[a] Military Technical Institute, Ratka Resanovića 1, Belgrade, Serbia
[b] Bundeswehr Institute of Pharmacology and Toxicology, Neuherbergstrasse 11, Munich, Germany
[c] National Institute of Chemistry, Hajdrihova 19, Ljubljana, Slovenia
[d] Faculty of Chemistry, University of Belgrade, Studentski Trg 12-16, Serbia
[e] Innovation Center of The Faculty of Chemistry, University of Belgrade, Studentski Trg 12-16, Serbia

ARTICLE INFO

Keywords:
Acetylcholinesterase
Irreversible inhibition
Nerve agents
Protection
Pre-treatment
Molecular dynamics simulations

ABSTRACT

Acetylcholinesterase (AChE) is an enzyme which terminates the cholinergic neurotransmission, by hydrolyzing acetylcholine at the nerve and nerve-muscle junctions. The reversible inhibition of AChE was suggested as the pre-treatment option of the intoxications caused by nerve agents. Based on our derived 3D-QSAR model for the reversible AChE inhibitors, we designed and synthesized three novel compounds **8-10,** joining the tacrine and aroylacrylic acid phenylamide moieties, with a longer methylene chain to target two distinct, toplogically separated anionic areas on the AChE. The targeted compounds exerted low nanomolar to subnanomolar potency toward the *E. eel* and human AChE's as well as the human BChE and showed mixed inhibition type in kinetic studies. All compounds were able to slow down the irreversible inhibition of the human AChE by several nerve agents including tabun, soman and VX, with the estimated protective indices around 5, indicating a valuable level of protection. Putative noncovalent interactions of the selected ligand **10** with AChE active site gorge were finally explored by molecular dynamics simulation suggesting a formation of the salt bridge between the protonated linker amino group and the negatively charged Asp74 carboxylate side chain as a significant player for the successful molecular recognition in line with the design strategy. The designed compounds may represent a new class of promising leads for the development of more effective pre-treatment options.

1. Introduction

Acetylcholinesterase (AChE, EC 3.1.1.7.) is a carboxylesterase which terminates cholinergic neurotransmission, by hydrolyzing the neurotransmitter acetyl-choline (ACh) in a synaptic cleft of nerve- and nerve-muscle junctions. Organophosphonates (OP), such as nerve agents used in terrorism and chemical warfare and organophosphates which are widely used as pesticides rapidly inactivate AChE by binding to the catalytic Ser203 leading to accumulation of ACh in the synaptic cleft and causing muscarinic (miosis, hypersalivation, bradycardia, diarrhea, bronchoconstriction), nicotinic (convulsions, muscle cramps and muscle dysfunction) and central signs and symptoms of intoxication, ultimately causing death by respiratory failure.

The currently approved treatment for the OP intoxication consists of anticholinergic drug, such as atropine, which relieves the muscarinic symptoms, an oxime, which is able, to some extent, to reactivate the irreversibly inhibited AChE and to restore its activity and an anticonvulsant drug (diazepam or its pro-drug avizafone) which is able to block nerve agent induced seizures. However, such treatment is not fully effective under life-threatening conditions [1]. The reasons for the ineffectiveness are diverse and multifaceted. Firstly, in order to be effective, the treatment has to be administered as soon as possible after exposure has happened, which can be rather complicated in the battlefield conditions. In the past several decades, numerous oximes have been synthesized and only two of them, pralidoxime (2-PAM) and obidoxime, are licensed and commercially available. Oximes are considered to be insufficiently efficient in case of soman poisoning, mainly due to rapid aging (*i.e.*dealkylation) of the nerve agent bound to the enzyme which prevents its reactivation. Also, tabun-inhibited AChE is highly resistant to reactivation [2,3]. Moreover, the two oximes, being

* Corresponding author.
E-mail address: mvitod@chem.bg.ac.rs (M.D. Vitorović-Todorović).

https://doi.org/10.1016/j.cbi.2019.06.027
Received 12 February 2019; Received in revised form 10 June 2019; Accepted 13 June 2019
Available online 19 June 2019
0009-2797/

a permanently positively charged species hardly cross blood-brain barrier (BBB), and reactivate CNS AChE to a low extent. Another drawback of 2-PAM is that a product of reactivation, phosphyl-oxime can readily re-inhibit enzyme [4,5].

Given the drawbacks of the above described standard treatment, the so-called 'pre-treatment' option was proposed. The pre-treatment is given to healthy individuals when there is a higher probability for chemical attack (which represents dilemma by itself). The pre-treatment usually consists of one or more following drugs: a pseudoirreversible, carbamate-type AChE inhibitor (pyridostigmine or physostigmine) and an anti-cholinergic drug (caramiphen, aprophen or scopolamine). The role of pseudoirreversible AChE inhibitor in the pre-treatment mixture is to temporarily inhibit fraction of the enzyme and protect it from irreversible inhibition by OP's. This might be especially important in case of soman intoxications where reactivation of AChE is impossible. One of the first carbamates tested for the pre-treatment is pyridostigmine. Several studies on experimental animals showed that pre-treatment with pyridostigmine or pyridostigmine/scopolamine mixture improves efficacy of the antidotal treatment after exposure to sarin or soman. However, this pre-treatment does not provide any protection when given alone, *i.e.*without any antidotal post-treatment [6–9]. The major drawback of pyridostigmine lies in the fact that it is permanently positively charged compound and it does not cross BBB, so it is unable to protect AChE in CNS. Thus, pre-treatment with physostigmine as an uncharged compound, able to cross BBB, was proposed along with different anticholinergic drugs. In the past two decades, several studies on experimental animals (Beagle dogs, rats and guinea pigs) consistently and convincingly demonstrated that pre-treatment with physostigmine when given in conjunction with anticholinergic drug (atropine, aprophen, scopolamine, procyclidine, benactyzine, etc.) *via* different administration routes (sustained release by mini-osmotic pumps, *i. v.* single dose, or *via* transdermal route) is able to afford considerable protection against multiple lethal doses of nerve agents including sarin, soman and VX and that physostigmine is far more superior as a pre-treatment comparing to pyridostigmine [8,10–13]. Another studies showed that huperzine A and galanthamine, the true reversible inhibitors of AChE, approved for the treatment of Alzheimer's disease, are also able to exert protective effects against nerve agent poisoning in experimental animals. Galanthamine was chosen for *in vivo* testing not only due to its mere anticholinesterase activity but also due to its additional advantages including BBB permeability, anticonvulsant properties and ability to prevent neurodegeneration. Albuquerque *et al.* showed that a single dose of galanthamine in combination with atropine is able to protect guinea pigs from the exposure to lethal doses of soman and sarin. Moreover, galanthamine was far more superior in preventing lethality comparing to accepted pre-treatment, pyridostigmine [14]. Similarly, it has been shown that huperzine A administered as a single dose or *s. c. via* osmotic pumps protects experimental animals (mice, non-human primates and guinea pigs) against toxic signs and lethality of soman [15]. Petroianu *et al.* also investigated and compared protection ability of eleven moderate to strong reversible AChE inhibitors (pyridostigmine, physostigmine, ranitidine, tiapride, tacrine, 7-metoxytacrine, amiloride, oxime K-27, metoclopramide and methylene blue) against paraoxone exposure in Wistar rats [16]. Study showed that the best protection from paraoxon-induced mortality was observed after pre-treatment with physostigmine and the oxime K-27, but pre-treatment with tacrine, pyridostigmine and ranitidine was also significant. All other compounds were ineffective or even had unfavorable effects.

Recently we performed a 3D-QSAR analysis based on alignment independent descriptors for the set of 110 structurally diverse AChE inhibitors [17]. The study included the so-called 'dual binding ligands' or 'dual inhibitors' which consisted of two structural cyclic aromatic fragments linked by a polymethylene chain. Such dual compounds were envisioned to simultaneously bind to two distinct sites on the AChE enzyme anionic site (AS), first one found deeper in the active site gorge and the second peripheral anionic site (PAS) which is located at the rim of the active site gorge.

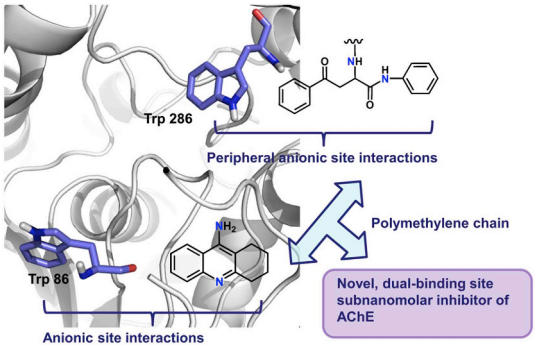

Fig. 1. Outline of the design strategy of „dual binding"compounds **8–10**: Compounds join the tacrine unit which strongly binds to the anionic site (AS) of AChE with the aroylacrylic acid phenylamide fragment which is a non-competitive low micromolar inhibitor of the enzyme with a flexible linker.

In this work, based on the literature data as well as the information obtained by the analysis of the most important outcomes from our QSAR models, we designed a set of dual binding compounds **8–10** which joined the tacrine and aroylacrylic acid amides fragments *via* an eight methylene linker as depicted in Fig. 1, to target two distinct topologically separated anionic areas on the AChE. Aroylacrylic acid amide fragment was included, because we previously confirmed its low micromolar activity and non-competitive mode of binding [18,19], and tacrine was included since it showed slightly better protective effects *in vivo* against the paraoxone intoxications than pyridostigmine [16]. The derived 3D-QSAR models suggested low nanomolar inhibitory activity of the designed compounds toward AChE. We synthesized such dual inhibitors, estimated their inhibitory activity toward AChE and other available cholinesterases and evaluated their *in vitro* protective effects against the irreversible inhibition of AChE by several nerve agents including tabun, soman and VX. Finally, the putative non-covalent interactions between the most active derivative and AChE were investigated by molecular dynamics to validate the design strategy. Such compounds could provide more effective pre-treatment options against nerve agents induced intoxications.

2. Materials and methods

2.1. Chemistry

All chemicals were purchased from Sigma Aldrich or Merck, and were used as received. The ^{1}H and ^{13}C NMR spectra were recorded in $CDCl_3$ on Varian Gemini 200/50 MHz or Bruker AVANCE 500/125 MHz instruments. Chemical shifts are reported in parts per million (*ppm*) relative to tetramethylsilane (TMS) as internal standard. Spin multiplicities are given as follows: *s* (singlet), *d* (doublet), *t* (triplet), *m* (multiplet), or *br* (broad). The HR-ESI-MS spectra were recorded on Agilent Technologies 6210-1210 TOF-LC-ESI-MS instrument in positive mode. Samples were dissolved in MeOH. The detailed procedures for the synthesis of aroylacrylic acid phenylamides are given elsewhere [18,19].

Synthetic procedure for **9-chloro-1,2,3,4-tethydro-aminoacridine** (**3**): The 16 mL of $POCl_3$ was carefully added to the mixture of anthranilic acid **1** (2.1 g, 15 mmol) and equimolar amount of cyclohexanone **2** in ice-bath. The mixture was heated under reflux for 2^{h}, then cooled at room temperature, and concentrated under reduced pressure to give slurry. The residue was diluted with EtOAc, neutralized with ice-cold aqueous K_2CO_3, and washed with brine. The organic layer was dried over anhydrous $MgSO_4$ and concentrated in vacuum to provide crude product, which was subsequently re-crystallized from acetone to give a final compound. ^{1}H NMR (200 MHz, $CDCl_3$) δ: 1.83–1.96 (*m*, 4H,

cyclohexyl–CH_2–); 2.93 (*t*, 2H, *J* = 5.63 Hz, cyclohexyl–CH_2–); 3.08 (*t*, 2H, *J* = 6.35 Hz, cyclohexyl–CH_2–); 7.47 (*t*, 1H, *J* = 7.06 Hz, *m*-phenyl); 7.62 (*t*, 1H, *J* = 6,77 Hz, *m*-phenyl); 7.95 (*t*, 1H, *J* = 8.19 Hz, *o*-phenyl); 8.09 (*t*, 1H, *J* = 7.06 Hz, *m*-phenyl). ^{13}C NMR (50 MHz, $CDCl_3$) *δ*: 12.42; 22.45; 27.28; 33.96; 123.46; 125.16; 126.17; 128.49; 129.05; 146.50; 159.26.

Synthetic procedure for ***N*-(1,2,3,4-tetrahidroacridine-9-yl)-octane-1,8-diamine** (**4**): The mixture of **3** (1 g, 4.61 mmol) and 1,8-diaminooctane (1.99 g, 13.8 mmol) in 1-penthanol (5 mL) was refluxed for 18^h at 160 °C. The mixture was cooled to room temperature and diluted with EtOAc (50 mL). The solution was washed with 10% NaOH aqueous solution, twice with distilled water, and dried with anhydrous $MgSO_4$. After the filtration of the dried solution, the solvent was removed under reduced pressure, and obtained semi-solid substance was purified by silica gel column chromatography ($CHCl_3$: MeOH: NH_4OH = 7: 3: 0.07). ^{1}H NMR (200 MHz, $CDCl_3$) *δ*: 1.13–1.19 (overlapped *m*, linker–CH_2–); 1.28 (*br*, 2H, linker–CH_2–); 1.47 (*br*, 2H, linker–CH_2–); 1.74 (*br*, 2H, cyclohexyl–CH_2–); 2.52 (*br*, 2H, cyclohexyl–CH_2–); 2.92 (*br*, 2H, linker–CH_2–); 3.03 (*br*, 2H, amino–NH_2–); 3.30 (*br*, 2H, linker–CH_2–); 3.84 (*br*, 1H, amino–NH–); 7.18 (*t*, 1H, *J* = 7.14 Hz, *m*-phenyl); 7.38 (*t*, 1H, *J* = 7.52 Hz, *m*-phenyl); 7.78–7.82(overlapped *m*, 2H, *o*-phenyl). ^{13}C NMR (50 MHz, $CDCl_3$) *δ*: 22.31; 22.58; 24.31; 26.36; 28.80; 31.22; 32.66; 33.52; 41.39; 48.91; 115.26; 119.75; 122.42; 122.98; 127.67; 128.15; 146.99; 150.27; 157.87.

General synthetic procedure for the target compounds **8–10**: To a mixture of aroyl-substituted (*E*)-4-aryl-4-oxo-2-butenoic acid phenylamide (7 mmol) in chloroform (15 mL), equimolar amount of **4** and 15 mL of toluene were added and the resulting mixture was stirred at room temperature for 24^h. The solvent was removed under reduced pressure, and obtained semi-solid substance was purified by silica gel column chromatography ($CHCl_3$: MeOH: NH_4OH = 7: 3: 0.07).

4-*N*-Diphenyl-4-oxo-2-[8-(1,2,3,4-tetrahydroacridin-9-ylamino)octylamino] butanamide (**8**): $C_{37}H_{44}N_4O_2$, reaction of (*E*)-4-phenyl-4-oxo-2-butenoic acid phenylamide (0.70 mmol) and equimolar amount of **4** gave **8** in quantitative yield as orange semi-solid.^{1}H NMR (200 MHz, $CDCl_3$) *δ*: 1.01–1.20 (overlapped *m*, 8H, linker–CH_2–); 1.50 (*br*, 2H, linker–CH_2–); 1.72 (*br*, 2H, linker–CH_2–); 2.51 (*br*, 4H, cyclohexyl–CH_2–); 2.90 (*br*, 4H, cyclohexyl–CH_2–); 3.33–3.40 (overlapped *m*, 7H, linker–CH_2– and ABX); 3.56–3.61 (*m*, 1H, ABX); 4.34 (*m*, 1H, ABX); 4.34 (*m*, 1H, ABX); 4.56 (*s*, amino–NH–); 4.89 (*s*, amino–NH–); 6.89–7.56 (overlapped *m*, tacrine-*m*-phenyl, amido-*p*-phenyl, amido-*m*-phenyl, aroyl-*p*-phenyl and aroyl-*m*-phenyl); 7.79–7.86 (overlapped *m*, 4H, aroyl-*o*-phenyl, amido-*o*-phenyl and tacrine-*o*-phenyl); 9.54 (*s*, 1H, amido-NH). ^{13}C NMR (50 Hz, $CDCl_3$) *δ*: 21.18; 22.23; 22.60; 24.35; 26.55; 26.84; 20.97; 29.90; 30.55; 31.37; 32.96; 41.57; 41.97; 43.05; 59.10; 61.38; 64.33; 67.15; 114.93; 119.13; 119.60; 122.03; 123.43; 124.34; 125.05; 126.67; 127.91; 128.78; 130.17; 135.99; 137.05; 137.56; 141.38; 142.14; 141.28; 151.10; 157.38; 170.15; 171.80; 196.49; 198.37. ESI-MS HR: 577.3529 (M + 1), Calc. 577.3537; 289.1807 (M + 2), Calc. 289.1805.

4-(4-Isopropylphenyl)-4-oxo-*N*-phenyl-2-[8-(1,2,3,4-tetrahydroacridine-9-ylamino)octyl-amino] -butanamide (**9**): $C_{40}H_{50}N_4O_2$, reaction of (*E*)-4-(4-isopropylphenyl)-4-oxo-2-butenoic acid phenylamide (0.70 mmol) and equimolar amount of **4** gave **9** in quantitative yield as orange semi-solid.^{1}H NMR (500 MHz, $CDCl_3$) *δ*: 1.23–1.25 (overlapped *m*, 8H, *d*, 2H, *J* = 7.09 Hz, *i*-PrCH_3); 1.31–1.37 (overlapped *m*, 8H, linker –CH_2-); 1.57 (*m*, 2H, linker–CH_2–); 1.64 (*m*, 2H, linker–CH_2–); 1.90 (*m*, 4H, cyclohexyl–CH_2–); 2.69 (*m*, 4H, cyclohexyl–CH_2–); 2.95 (*h*, 1H, $J_{1,2}$ = 6.59 Hz, $J_{1,3}$ = 13.78 Hz, *i*-PrCH); 3.05 (*br*, 2H, linker–CH_2–); 3.28 (*dd*, 1H, $J_{1,2}$ = 8.19 Hz, $J_{1,3}$ = 17.38 Hz, ABX); 3.47 (*t*, 2H, *J* = 7.39 Hz, amino-NH); 3.62 (*dd*, 1H, $J_{1,2}$ = 3.20 Hz, $J_{1,3}$ = 17.39 Hz, ABX); 3.70 (*dd*, 1H, $J_{1,2}$ = 3.64 Hz, $J_{1,3}$ = 8.71 Hz, ABX); 7.09 (*t*, 1H, *J* = 7.47 Hz, amido-*p*-phenyl); 7.29–7.34 (overlapped *m*, 6H, amido-*m*-phenyl, amido-*o*-phenyl and tacrine-*m*-phenyl); 7.58 (*d*, 2H, *J* = 7,64 Hz, aroyl-*m*-phenyl); 7.91 (*d*, 2H, *J* = 8.28 Hz, tacrine-*o*-phenyl); 7.95 (*d*, 2H, *J* = 8.28 Hz, aroyl-*o*-phenyl); 9.60 (*s*, 1H, amido-NH). ^{13}C NMR (125 Hz, $CDCl_3$) *δ*: 22.70; 22.96; 23.55; 24.71; 26.82; 27.08; 29.26; 30.15; 31.69; 33.86; 34.21; 40.04; 48.37; 49.44; 59.45; 115.72; 119.24; 120.12; 122.82; 123.52; 124.04; 126.77; 128.27; 128.41; 128.52; 128.94; 134.12; 137.73; 147.31; 150.80; 155.21; 158.30; 171.90; 196.18. ESI-MS HR: 310.2046 (M + 2), Calc. 310.2045.

4-(3,4-Dimethylphenyl)-4-oxo-*N*-phenyl-2-[8-(1,2,3,4-tetrahydroacridin-9-ylamino)octyl-amino] -butanamide (**10**): $C_{39}H_{48}N_4O_2$, reaction of (*E*)-4-(3,4-dimetylphenyl)-4-oxo-2-butenoic acid phenylamide (0.70 mmol) and equimolar amount of **4** gave **10** in quantitative yield as orange semi-solid.^{1}H NMR (500 MHz, $CDCl_3$) *δ*: 1.25–1.37 (overlapped *m*, 8H, linker–CH_2–); 1.50 (*m*, 2H, linker–CH_2–); 1.64 (*m*, 2H, linker–CH_2–); 1,90 (*m*, 4H, cyclohexyl–CH_2–); 2.29 (*s*, 3H, –CH_3); 2.30 (*s*, 3H, –CH_3); 2.69 (*m*, 4H, cyclohexyl–CH_2–); 3.06 (*m*, 4H, linker–CH_2–); 3.26 (*dd*, 1H, $J_{1,2}$ = 8.70 Hz, $J_{1,3}$ = 17.40 Hz, ABX); 3.47 (*t*, 2H, *J* = 7.15 Hz, amino–NH–); 3.62 (*dd*, 1H, $J_{1,2}$ = 4.35 Hz, $J_{1,3}$ = 17.39 Hz, ABX); 3.68 (*dd*, 1H, $J_{1,2}$ = 4.35 Hz, $J_{1,3}$ = 8.70 Hz, ABX); 7.09 (*t*, 1H, *J* = 7.14 Hz, amido-*p*-phenyl); 7.13–7.25 (overlapped *m*, 3H, amido-*m*-phenyl, aroyl-*m*-phenyl); 7.32 (*m*, 2H, amido-*o*-phenyl); 7.53 (*t*, 1H, *J* = 6.88 Hz, tacrine-*m*-phenyl); 7.59 (*d*, 1H, *J* = 8.35 Hz, aroyl-*o*-phenyl); 7.70 (*t*, 1H, *J* = 7.37 Hz, tacrine-*m*-phenyl); 7.74 (*s*, 1H, aroyl-*o*-phenyl); 7.91 (*d*, 1H, *J* = 8.35 Hz, tacrine-*o*-phenyl); 7.95 (*d*, 1H, *J* = 7.86 Hz, tacrine-*o*-phenyl); 9.59 (*s*, 1H, amido-NH). ^{13}C NMR (125 Hz, $CDCl_3$) *δ*: 19.70; 20.00; 21.39; 22.70; 22.99; 24.71; 26.77; 27.09; 29.27; 30.16; 31.69; 33.87; 40.12; 48.38; 49.44; 59.50; 115.70; 119.23; 120.11; 122.79; 123.54; 124.03; 125.23; 125.88; 128.57; 128.94; 129.25; 129.91; 134.17; 137.05; 137.76; 143.25; 147.27; 150.82; 158.25; 171.95; 198.39. ESI-MS HR: 605.3830 (M + 1), Calc. 605.3856; 303.1967 (M + 2), Calc. 303.1967.

2.2. Biological studies

2.2.1. Reversible inhibition of E. Eel AChE

The inhibition potency of the compounds **8–10** toward *E. Eel* AChE was evaluated by Ellman procedure [20], using the type VI-S enzyme (Sigma) and acetylthiocholine iodide (0.28 mM) as a substrate. Broad range of concentrations, which produce 20–80% of enzyme activity inhibition, were used for each compound. The reaction took place in the final volume of 2 mL of 0.1 M potassium phosphate buffer, pH 8.0, containing 0.03 units of AChE and 0.3 mM 5,5-dithio-bis(2-nitrobenzoic)acid (DTNB), used to produce yellow anion of 5-thio-2-nitrobenzoic acid in reaction with thiocholine released by AChE. Tested compound was added to the enzyme solution and preincubated at 25 °C for 15 min, followed by the addition of DTNB (0.1 mL) and substrate (0.05 mL). Determination of inhibition curves were performed at least in triplicate. One triplicate sample without test compound was always present to yield 100% of AChE activity. The reaction was monitored for 0.5 min (absorbance was measured every 10 s), and the color production was measured at 412 nm. The reaction rates were compared, and the percent of inhibition, due to the presence of test compounds, was calculated. IC_{50} values were obtained by fitting the data into dose-response curves (inhibitor concentration *vs*. velocity of enzyme reaction), according to formula:

$$\frac{v_i}{v_0} = \frac{1}{1 + ([I]/IC_{50})^h}$$

where v_i and v_o are initial velocities of the enzyme reaction in the absence and in presence of inhibitor, [I] is inhibitor concentration and h is the Hill coefficient.

From dose-response experiments we were able to determine Hill coefficient and to estimate the possible cooperative effects during the process of inhibitor binding.

The inhibition reaction was also monitored continuously during 15 min after the initiation of the reaction in order to determine the time interval which is needed to achieve equilibrium of the reversible inhibition reaction.

For the estimation of the inhibition type, Lineweaver-Burk plots were generated by using the fixed amount of acetylcholinesterase and

varying amounts of the substrate (0.097–0.582 mM), in the absence and in the presence of different inhibitor concentrations. The re-plots of the slopes and intercepts of the double reciprocal plots against inhibitor concentrations gave the inhibitor constants (K_{i1} and K_{i2}, for the binding to free enzyme and enzyme substrate complex correspondingly) as the intercepts on the x-axis.

2.2.2. Reversible inhibition of native HuAChE and HuBChE

Acetylthiocholine iodide (ATCh), *S*-butyrylthiocholine iodide (BTCh), 5,5′-dithio-bis-2-nitrobenzoic acid (DTNB) and isolated human butyrylcholinesterase (BChE) were purchased from Sigma Aldrich (Taufkirchen, Germany). All other chemicals were purchased from Merck Eurolab GmbH (Darmstadt, Germany) at the purest grade available. Processing of experimental data was performed by linear and non-linear regression analysis using line and curve fitting programs provided by GraphPad Prism 5.0 (GraphPad Software, San Diego, Calif. USA). All experiments were carried out at a minimum of n = 2 and data were expressed as mean ± SD.

Haemoglobin-free human erythrocyte membranes ('ghosts') were prepared from human whole blood and served as source of human erythrocyte AChE [21]. Aliquots of erythrocyte ghosts were adjusted to the original whole blood AChE activity and stored at −80 °C. Prior to use, aliquots were thawed gently and homogenized on ice using a Sonoplus HD 2070 ultrasonic homogenator (Bandelin electronic, Berlin, Germany), three times for 5 s with 30-s intervals to obtain a homogeneous matrix for kinetic analysis.

A modified Ellman procedure was used [20,22] to determine the AChE and BChE activity spectrophotometrically (Cary 50 Bio UV/Visible Spectrophotometer) at 412 nm using polystyrol cuvettes with 0.45 mMATCh (AChE) and 1 mMBTCh (BChE) as substrate and 0.3 mM DTNB as chromogen in 0.1 M phosphate buffer (pH 7.4). All measurements were performed at least in duplicate at 37 °C and pH 7.4. The IC_{50} was measured at a fixed substrate concentration using different compound concentrations (0.1–1000 μM). In brief, 10 μL erythrocyte ghosts or BChE and 3.2 μL compound were added to a cuvette prefilled with phosphate buffer and DTNB. After adding ATCh or BTCh, the enzyme activity was continuously monitored for up to 3 min and IC_{50} values were calculated from semi-logarithmic dose-response curves of the ligand concentration versus AChE/BChE activity.

The time dependence of inhibition was determined by incubating human AChE and BChE with compounds **8**, **9** or **10** (500 nM) and the AChE/BChE activity was determined after 1, 7 and 15 min. The reversibility of inhibition of human AChE and BChE was tested by incubating enzyme solutions with appropriate compound concentrations (AChE: 300 nM compounds **8** and **9**, 10 nM compound **10**; BChE: 100 nM compounds **8** and **9**, 50 nM compound **10**) for 5 min, followed by extensive dilution (300 fold) and determination of AChE/BChE activity. All enzyme activities were referred to untreated control activities.

*2.2.3. Tabun, soman and VX inhibition kinetics with human AChE in the absence and presence of compounds **8–10***

The organophosphorus compounds (OP) tabun (*O*-ethyl *N*,*N*-dimethylphosphoroamidocyanidate), soman (*O*-pinacolyl methylphosphonofluoridate) and VX (*O*-ethyl *S*-2-diisopropylamino-ethylmethyl phosphonothiolate) (> 95% by GC-MS, ^{1}H NMR and ^{31}P NMR) were made available by the German Ministry of Defence. OP stock solutions (0.1% v/v) were prepared in acetonitrile, stored at 20 °C and appropriately diluted in distilled water just before use. Stock and working solutions of compounds **8–10** were prepared in methanol.

The effect of the tested compounds on the time-dependent inhibition of human AChE by tabun, soman and VX was tested by mixing the native human AChE with compounds **8** (100 nM), **9** (100 nM) and **10** (5 nM), immediately followed by the addition of tabun (50 nM), soman (10 nM) or VX (10 nM). After 1–20 min, aliquots were taken and the residual AChE activity was determined (n = 2).

The inhibition kinetics of tabun, soman and VX was determined with human AChE in the presence of the substrate ATCh: 10 μL native AChE (the estimated AChE concentration in the cuvette was ~20 pM) and 5 μL diluted OP (8 different concentrations; tabun: 150–500 nM, soman: 10–70 nM, VX: 20–130 nM)) were added to pre-heated cuvettes, containing 3000 μL phosphate buffer (0.1 M, pH 7.4), 100 μL DTNB and 50 μL ATCh (final volume 3165 μL). ATCh hydrolysis was continuously monitored for 5 min. The inhibition kinetics were determined in the absence or presence of compounds **8** (20 and 100 nM), **9** (30 and 100 nM) and **10** (1 and 5 nM). The recorded curves were analyzed by non-linear and linear regression analysis according to Forsberg and Puu in order to calculate the second order inhibition rate constants k_i [23,24]. The protective index (PI) was calculated by dividing the k_i in the absence by the k_i in the presence of compounds **8**, **9** or **10**.

*2.2.4. Reactivation of sarin-inhibited AChE by HI-6 in the absence or presence of compounds **8–10***

HI-6 (1-[[[4-(aminocarbonyl)-pyridinio]-methoxy]methyl]-2-[(hydroxyimino)methyl]pyridinium dichloride monohydrate) was provided by Dr. Clement (Defence Research Establishment Suffield, Ralston, Alberta, Canada). Sarin-inhibited human AChE was incubated with 10 μM HI-6 in the absence or presence of compounds **8** (20 and 100 nM), **9** (30 and 100 nM) and **10** (1 and 5 nM). Aliquots were taken after 2–60 min to determine AChE activities which were referred to the activity of native AChE and the % reactivation was calculated. The pseudo-first order reactivation rate constant k_{obs} was calculated by non-linear regression analysis.

2.3. Molecular modelling study

The initial coordinates of AChE enzyme were taken from the PDB database (entry 4EY4) [25]. The missing residues were added using SwissPDB web server [26]. All co-crystallized ligands, ions and water molecules were removed. The 3D conformation of ligand **10** used for molecular docking was generated using MMFF94 force field [27] and reoptimized using semiempirical PM7 method [28]. The protonation state of ligand and protein were set at pH 7.4, as predicted by PROPKA [29]. The binding site was defined as all residues in the 13 Å sphere around Tyr340, comprising both deep-pocket active site residue Trp86 and peripheral site residue Trp286, as well as other residues important for binding of AChE inhibitors. AutoDockVina [30] and PLANTS [31] were used for docking the ligand into the AChE active site. AutoDockVina exhaustiveness parameter was set to 250 while other parameters were default. Vega ZZ 3.1.0 [32] was used as GUI for all docking calculations.

The best docking solution of compound **10** from the AutoDockVina calculation was further used for the molecular dynamics simulation using NAMD MD engine. CHARMM-GUI [33] was utilized for the preparation and solvation of the protein-ligand complex, adding an octahedral cluster of TIP3 water molecules at 10 Å from the edge. The solvated system was neutralized by placing the 7 potassium ions using Monte Carlo method. CHARMM36 m [34] force field parameters were used, while the atomic types and partial charges for ligand were assigned using CHARMM General Force Field (CGenFF) [35](see Fig. S1 for assigned ligand **10** parameters). The final system consisted of 48334 atoms and the necessary NAMD simulation files were generated using CHARMM-GUI. All MD calculations were performed on the GPU cluster at the National Institute of Chemistry, Ljubljana.

NAMD 2.11 engine [36] was used for the MD calculations using the following settings. All 1–3 and modified 1–4 interactions were accounted by specifying "exclude scaled 1-4" keyword. Periodic boundary conditions were specified based on the size of the full solvated system. Initial minimization of the system was performed to remove the steric bumps followed by a 500 ps MD equilibration with a 2 fs step using the Nose-Hoover Langevin piston pressure of 1 atm at the 303.15 K. Electrostatics was treated with the Particle mesh Ewald (PME) algorithm, with the cut-off distance for the non-bonded interactions set to 12 Å,

switch distance at 10 Å, and storing all pairs within 16 Å (pairlistdist = 16). After equilibration, 100 ns of production through unconstrained, Langevin MD simulation was performed using a 2 fs integration step.

For the MD trajectory analysis, 1000 equidistant frames were extracted from the trajectory, and aligned using the RMSD Trajectory Tool in VMD [37]. Interaction energy analysis was performed using NAMD Interaction energy tool available in VMD. The RMSD, RMSF, gyration radius, distances and other geometric parameters were explored using VMD and VEGA ZZ.

To further provide a more comprehensive outlook of the observed dynamical interaction pattern between the simulated ligand **10** and the AChE binding site, 1000 exported MD frames were used in the dynamic pharmacophore analysis using DynophoreApp framework developed in the group of Prof. Gerhard Wolber with default settings [38,39]. Dynophores were subsequently visualized within the LigandScout program [40]. These calculations yielding a dynophore model and corresponding output files were performed on the computers of the Molecular Design Lab at the Freie Universität Berlin, Germany and subsequently visualized in LigandScout.

3. Results and discussion

3.1. Chemistry

Synthetic path to compounds **8–10** is given in Fig. 2. The Niementowski reaction between 2-aminobenzoic (anthranilic) acid and cyclohexanone proceeded smoothly to give **3**. The presence of 9-chloro substituent on the molecule enabled further functionalization of the compounds. The nucleophilic aromatic substitution of 9-chloro substituent of **3**, by using triple molar amount of linker (1,8-diaminooctane) gave exclusively monomeric product **4**. Michael's addition of **4** on correspondingly substituted aroylacrylic acid amide gave target compounds **8–10**. Synthesized compounds were characterized by ^{1}H and ^{13}C NMR spectroscopy and by high resolution mass spectrometry with electrospray ionization (ESI-HR-MS). The ^{1}H and ^{13}C NMR spectra of **8–10** are given in Supplementary material (Figs. S2–S7).

3.2. Biological studies

3.2.1. Inhibition potency of *8–10* toward EeAChE, HuAChE and HuBChE

Inhibition potency of compounds **8–10** determined toward *Ee*AChE, *Hu*AChE and *Hu*BChE is given in Table 1 and dose-response curves for

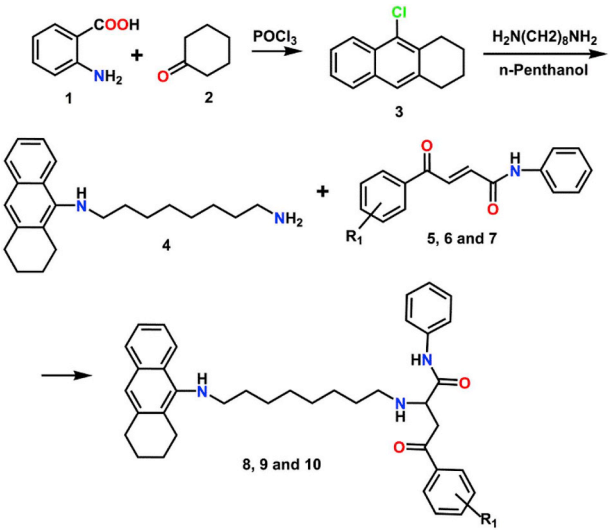

Fig. 2. Synthetic path to compounds **8** (R_1 = H) **9** (R_1 = 4-*i*-Pr) and **10** (R_1 = 3,4-diMe).

*Hu*AChE and *Hu*BChE inhibition are provided in Fig. 3. All three compounds are highly potent low nanomolar inhibitors of all three cholinesterases. The more potent inhibitors are compounds which have no substituents on the aroyl-phenyl ring (**8**) or have small substituents such as methyl groups on the aroyl-phenyl ring (**10**). Compound **9**, with a more voluminous isopropyl group has slightly higher IC_{50} value toward both electric eel and human AChE. It has been proven in a number of previous studies that dual AChE inhibitors bind in the way in which the tacrine substructure is oriented toward the bottom of the active site gorge, interacting with Trp86 and Tyr337 AS residues, while the other, usually aromatic and polycyclic fragment of the molecule is oriented toward the entrance of the active site gorge and interacts with amino acid residues that belong to PAS namely Trp286, among others.

The finding that compound **9** exerts slightly lower inhibition potency, compared to compounds **8** and **10** was unexpected, since it is well known that PAS area of the enzyme is wide and can accommodate a variety of highly voluminous molecular fragments. However, it is possible that aroylacrylic acid amide fragment of **9**, bearing a 4-*i*-Pr substituent, experience some steric hindrance upon binding to PAS and therfore tacrine moiety is unable to fully reach an AS of AChE, which results in slightly lower potency.

Subsequently, we tested the velocity of reaching equilibrium for the reversible inhibition, by following the residual enzyme activity in longer period of time (15 min) after the initiation of the inhibition reaction. The equilibrium is reached almost instantly and residual enzyme activity was constant during the remaining reaction time (*results not shown*). The inhibition of *Hu*AChE and *Hu*BChE was also fully reversible as tested by the dilution experiments. Therefore, we can state that three synthesized novel compounds (**8**, **9** and **10**) represent true, fast and highly potent reversible inhibitors of both AChE and BChE.The inspection of the Hill's coefficients (Table 1), showed that all three compounds have the value of coefficients around 1.0, which indicates almost no cooperativity in the ligand binding to the four subunits of the *E. eel* AChE tetramer.

We also determined the inhibition type for the compounds **9** and **10** by following the enzyme reaction at several different substrate concentrations, for the two fixed inhibitor concentrations. The inhibition constants and types are shown in Table 2, along with the corresponding double-reciprocal Lineweaver-Burk plots in Fig. 4. From the inspection of the Lineweaver-Burk plots compounds **9** and **10** are noncompetitive inhibitors and bind both to the free enzyme and the enzyme intermediate formed during substrate hydrolysis, which is evident from the intersection of the lines in the upper left quadrant.

3.2.2. Tabun, soman and VX inhibition kinetics with the human AChE in the absence and presence of compounds *8–10*. Protective effects of *8-10* against irreversible inhibition by nerve agents

We examined the inhibition kinetics with the three nerve agents tabun, soman and VX in the absence and in the presence of compounds **8–10**, in order to calculate the protective index (PI) of reversible inhibitors against irreversible inhibition by the nerve agents. Two concentrations of **8–10** were used and the results are given in Fig. 5 (left panel).

The experiments revealed that under the experimental conditions applied for the determination of the second order inhibition rate constants the compounds were able to protect AChE from inhibition by nerve agents partially at high compound concentrations, *i.e.* 100 nM of compounds **8** and **9** and 5 nM of compound **10**, resulting in a PI of up to 6 (Fig. 5 left panel). At lower compound concentrations (*i.e.* 20 nM compound **8**, 30 nM compound **9**, 1 nM compound **10**), being slightly above the respective IC_{50} values, the effect was only marginal. It was also interesting to note that different compounds, although quite similar in structure and the mode of reversible inhibition, provided different protection against different organophosphates.

The protective index (PI) was calculated by dividing the second order rate constant k_i in the absence by the k_i in the presence of

Table 1
Inhibition potency of compounds **8–10** toward *Ee*AChE, *Hu*AChE and *Hu*BChE.

No.		*Ee*AChE		*Hu*AChE	*Hu*BChE
	R1	IC_{50} ± SEM (nM)	Hill's coeff.	IC_{50} ± SD (nM)	IC_{50} ± SD (nM)
8	-H	7.76 ± 0.34	1.09 ± 0.08	18.7 ± 0.2	4.4 ± 0.1
9	-4-*i*-Pr	15.61 ± 1.12	1.05 ± 0.08	27.1 ± 0.1	8.0 ± 0.01
10	−3,4-diMe	5.24 ± 0.41	1.24 ± 0.16	0.66 ± 0.01	2.0 ± 0.01

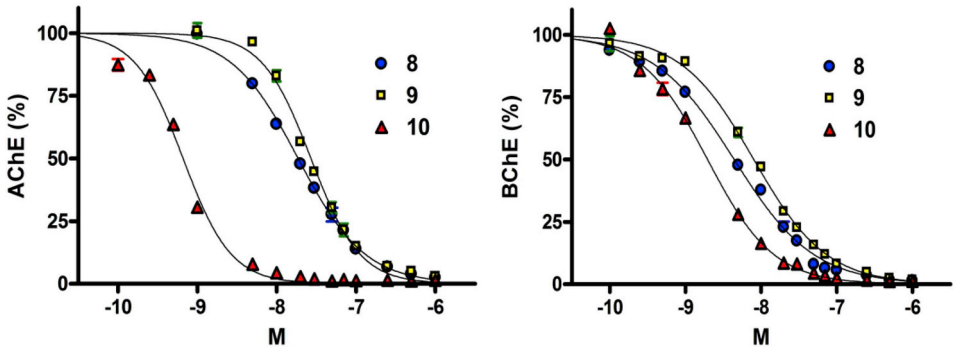

Fig. 3. Concentration-dependent inhibition of the human AChE and BChE by compounds **8–10**. Fourteen different compound concentrations ranging from 0.1 to 1000 μM were tested. Data were presented as % AChE activity and expressed as mean values ± SD of two independent experiments.

Table 2
The inhibition constants for the binding to free enzyme (K_{i1}) and enzyme intermediate formed during substrate hydrolysis (K_{i2}) for the **9** and **10**, and corresponding inhibition types.

Comp	K_{i1} (nM)	K_{i2} (nM)	Inh. Type
9	7.45	9.26	noncompetitive
10	4.46	9.18	noncompetitive

compounds **8**, **9** or **10**. According to the experimental protocol, the k_i values were calculated from the inhibition curves recorded for 5 min. Hence, it was tempting to test whether the test compounds are able to reduce the inhibition of human AChE by the nerve agents over a prolonged time (Fig. 5 right panel). In fact, compounds **8** and **9** (100 nM) were able to slow down the inhibition by tabun (50 nM), soman (10 nM) and VX (10 nM) and to preserve a small portion of AChE from the irreversible inhibition after 20 min. In contrast, compound **10** (5 nM) failed to preserve AChE from phosphylation.

Based on the current available literature data, it is difficult to estimate whether the achieved protective effects would be significant *in vivo*. The most abundant *in vivo* data are those on animal models which investigated protective effects of FDA approved AChE reversible inhibitors (galanthamine and huperzine A) with known ADME-Tox properties. However, *in vitro* data for the protective indices for these compounds are not published.

Various studies investigated reversible AChE inhibitors *in vitro*, but for those compounds *in vivo* data on animal models are scarce. For instance, Radić et al. [41] investigated the effects of several peripheral site reversible AChE inhibitors (gallamine, D-tubocurarine, propidium, atropine, coumarine derivatives) on rates of irreversible AChE inhibition by several organophosphate compounds, including paraoxon, haloxon, DDVP and neutral and cationic alkylmethylphosphonylthioates. Interestingly, most of the peripheral site reversible inhibitors actually increased the rates of the irreversible inhibition for about 6-fold in submilimolar concentrations while at higher concentration decreased the constants of irreversible inhibition but in the best cases to the level of the constants without reversible inhibitor present. Therefore, neither of these peripheral site ligands affords any protection *in vitro*. Petroianu et al. [42–44] investigated the effects of several moderately potent reversible AChE inhibitors including metoclopramide, ranitidine and L-lactate on the rates of irreversible inhibition by organophosphate pesticides paraoxon and mipafox. The protective effects were estimated in the terms of IC_{50} shift for paraoxon in the presence and in the absence of AChE reversible inhibitors, which are not comparable to our data for PI. Although these reversible inhibitors provided some level of *in vitro*

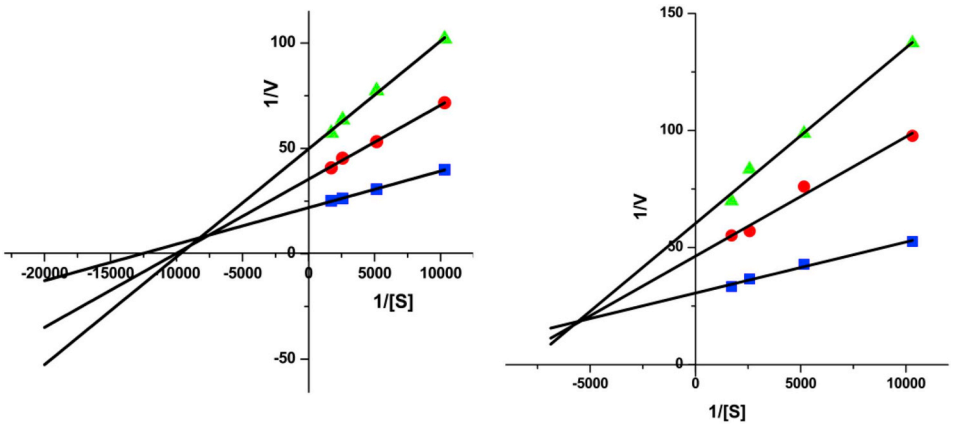

Fig. 4. Left: Lineweaver-Burk plot of AChE (0.03 U) in the absence and in the presence of different concentration of **9**: blue squares - no inhibitor, red dots – 6.3 nM and green triangles – 12.6 nM. Right: Lineweaver-Burk plot of AChE (0.03 U) in the absence and in the presence of different concentration of **10**: blue squares - no inhibitor, red dots – 3.97 nM and green triangles – 7.94 nM.

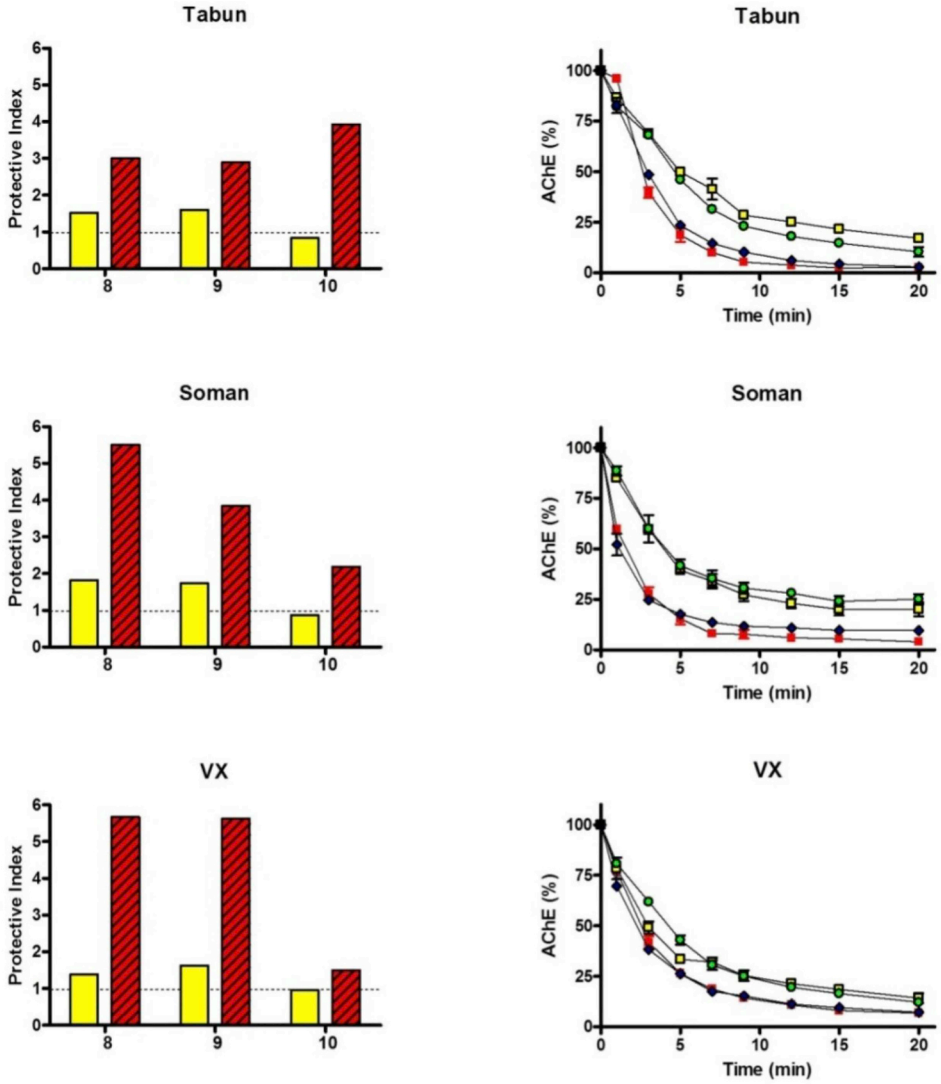

Fig. 5. Left panel: Protective index (PI) of compounds **8–10** for the inhibition of human AChE by tabun, soman and VX. The inhibition kinetics of tabun (150–500 nM), soman (10–70 nM) and VX (20–130 nM) was determined with human AChE in the presence of the substrate ATCh and the absence and presence of compounds **8–10**. The protective index (PI) was calculated by dividing the k_i in the absence by the k_i in the presence of compounds **8**, **9** or **10**. Yellow columns: 20 nM compound **8**, 30 nM compound **9**, 1 nM compound **10**; red hatched columns: 100 nM compounds **8** and **9**, 5 nM of compound **10**. Right panel: Effect of compounds **8** (yellow squares; 100 nM), **9** (green dots; 100 nM) and **10** (blue romboids; 5 nM) on the time dependent inhibition of human AChE by tabun (50 nM), soman (10 nM) and VX (10 nM).

protection, only ranitidine was tested *in vivo* [45]. The 30 min administration of ranitidine before exposure to paraoxon increased survival of male Wistar rats, but the effects were far better with pyridostigmine. Taking all of above into consideration, it might be concluded that compounds **8–10** showed moderate level of protection of AChE against irreversible inhibition by nerve agents and might be a promising leads for the development of more effective protective agents.

The effects of compounds **8–10** on the sarin-inhibited AChE reactivation by oxime HI-6 were also tested (*results not shown*). All three compounds had neither beneficial nor detrimental effects on enzyme reactivation. The reason for the lack of the effect of impairment *i.e.* decrease in the reactivation reaction is probably due to a high concentration of HI-6 (10 μM) and low concentration of compounds **8**, **9** and **10** that were used in the assay.

3.3. Molecular modelling of the inhibitor *10*-AChE molecular recognition

After firmly establishing the AChE inhibition of the synthesized derivatives, molecular dynamics simulations (MD) provided further valuable insights into the possible molecular recognition between the most active derivative, compound **10** and AChE active site gorge residues. Thus, the selected docked binding mode of compound **10** was subsequently simulated in the 100 ns long MD simulation, using NAMD suite of programs. Subsequently, 1000 equidistant MD frames were exported and analyzed, and the percentage of the occurrence of each interaction between the ligand structural motifs and AChE residues was calculated. Compound **10** was simulated with the protonated distal linker –NH- group which is near the aroylphenylamide fragment of the molecule, as estimated by the PROPKA program. The proximal linker –NH- group, as well as the tacrine pyridine nitrogen, were estimated as being unprotonated and thus were modelled as uncharged.

The gyration radius of the whole protein was found to be in the range between 20.9544 and 23.2942 with an average value of 22.8296 ± 0.2636 and remained stable during the MD simulation, indicating a stable folding of the protein structure (Fig. S8, Supplementary material). After the initial conformational change observed during the first 10 ns of production stage, the protein's conformation was stable as indicated by RMSD of protein's backbone (Fig. S9, Supplementary material). The movie, obtained from the trajectory showing a representative behavior of the protein ligand-system is also provided as Supplementary material, Video 1.

Supplementary video related to this article can be found at https://doi.org/10.1016/j.cbi.2019.06.027

The exported frames of the MD trajectory were then analyzed using the dynamic pharmacophore-Dynophore approach [38,39]. This provided a broader, more general overview opposed to the usual MD analysis which is typically directed to analyzing selected distances of the observed intermolecular interaction pattern during the MD trajectory. With dynophores we were able to evaluate the importance, occurrence and spatial evolution of the chemical interactions in terms of

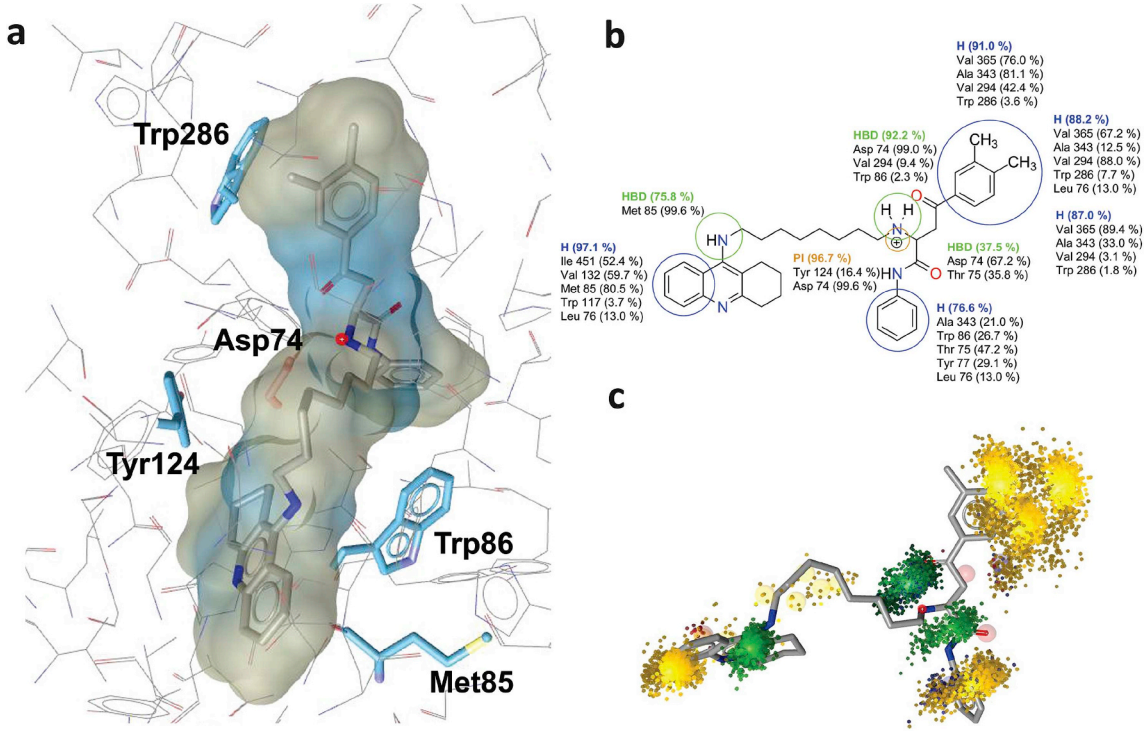

Fig. 6. (a) The observed intermolecular interactions between the compound **10** (grey sticks) and AChE. Ligand molecular surface is indicated. The carbon atoms of the important interacting residues are colored blue, while electrostatically bonded Asp74 is colored as red sticks; (b) Schematic representation of the results of the dynophore analysis for binding of the protonated ligand **10** to the AChE. The percentage of occurrence of each pharmacophore feature (H-hydrophobic, HBD-hydrogen bond donating, and PI- positive ionizable) is shown, along with theAChE active site residues forming each interaction; (c) Determined dynophore model showing the interaction pharmacophore features of compound **10** throughout MD simulation. Hydrophobic interactions are shown as yellow, HBD as green and PI as red spheres.

pharmacophore elements associated with a certain interaction while concurrently identifying the involved interaction residues [46]. The most important observed intermolecular interactions between the compound **10** and AChE residues, as a result of dynophore analysis are given in Fig. 6.

At the beginning of the MD simulation, the obtained ligand **10** docked conformation stretched between the two main sites in the AChE gorge: the anionic site (AS), found almost at the bottom of the gorge and comprising Trp86 residue, and the peripheral anionic site (PAS), found at the rim of the gorge and comprising Trp286 residue. At this starting docking position, tacrine moiety and the phenylamide ring of the aroylacrylic acid phenylamide moiety were found near the Trp86 indole ring. However, during the first 5 ns of the simulation, the tacrine fragment of the ligand protruded more deeply into the active site of the enzyme and occupied the hydrophobic pocket formed by Ile451, Val132, Met85 and Leu130 residues (Fig. 6a and b).

The dynophore analysis revealed that hydrophobic interactions of the tacrine phenyl ring with Met85 with the occurrence of 80.5% and Val132 with occurrence 59.7% are the most prominent and most stable during the simulation. Next, the proximal linker –NH- group forms a strong hydrogen bond with the backbone oxygen of Met85 (Fig. 7c) and this interaction remained stable and present during the whole trajectory. Interestingly, no hydrophobic interactions were observed for the polymethylene chain linker.

When analyzing the distal part of the molecule, *i.e.* aroylacrylic acid phenylamide part, several important interactions were detected. Phenylamide ring is situated near the anionic site of the enzyme and forms hydrophobic interactions most of the MD simulation (76.6%) with several residues including: Ala343, Trp86, Tyr77, Leu 76 and Thr75. The stacking interaction between phenylamide ring and Trp86 indole ring was also observed (Fig. 7b). Dimethylaroyl ring of the distal part of the molecule, in the first 5 ns of the simulations shifted away from the Trp286 indole ring toward the hydrophobic pocket formed by Val365, Ala343 and Val294 residues. Such observed behaviours confirmed the importance of the postdocking analysis of the suggested binding modes to provide deeper insight in the molecular recognition [47]. Hydrophobic interactions between these residues and 3,4-dimethylphenyl ring were stable during the whole trajectory with the occurrence above 80%. The ionic interaction, the salt bridge between the protonated linker –NH- group and negatively charged Asp74 carboxylate side chain was also identified. Although Asp74 is part of the flexible "Ω-loop" of AChE, this interaction is present during the whole simulation with the high occurrence of 99.6% (Figs. 6b and 7a). However, two temporary shifts (increase) in the distance have been observed around 17th and 92nd ns of simulation.

We also determined the interaction energy between the simulated ligand **10** and AChE and the energy graph is shown in Fig. 7a. The overall interaction energy remained stable with the electrostatic component predominantly connected with the Asp74 - charged amino linker having a bigger contribution that the van der Waals interactions. Furthermore, the sharp drop in electrostatic energy nicely geometrically corresponds to the temporary shift of Asp74 away from the positively charged linker –NH- group. It also confirms that this ionic interaction indeed provides a significant contribution to the total energy of the complex formation. The non-polar interaction contribution was still considerable owing to the many hydrophobic interactions observed between the compound **10** and the surrounding residues (Fig. 6b). These interactions remained stable throughout the trajectory.

4. Conclusions

In the present study, by utilizing previously derived 3D-QSAR model we designed and synthesized three novel AChE reversible "dual binding" inhibitors **8-10** joining the tacrine and aroylacrylic acid

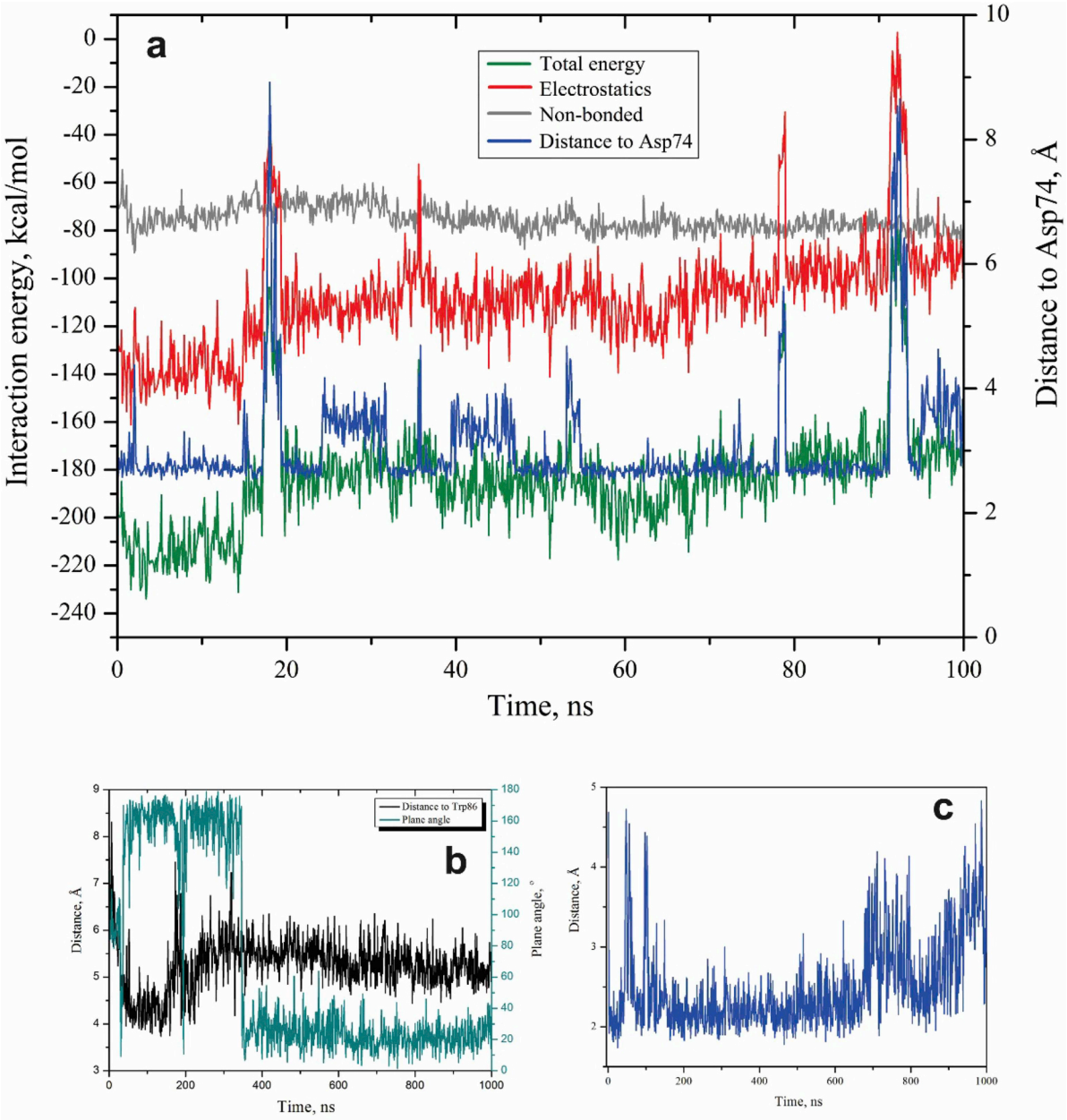

Fig. 7. Selected geometric and energetic parameters of the MD simulation: (a) Interaction energy between **10** and AChE during the 100 ns MD simulation. Electrostatic component of the total energy correlates with the distance between Asp74 and positively ionized N atom of linker. The average distance between Asp74 and **10** is 3.05 ± 0.81 Å. (b) Observed stacking interaction between aniline ring of **10** and indole ring of Trp86. (c) Hydrogen bond interaction between the linker NH proximal to tacrine moiety and backbone oxygen from Met85. The average distance is 2.50 ± 0.55 Å.

phenylamide structural fragments with a flexible linker. In our design strategy these two moieties targeted two distinct AChE interaction sites - anionic site deep inside the active and the peripheral anionic site located outside of the main binding gorge on the enzyme. All compounds displayed potent low nanomolar to subnanomolar inhibition potency toward several cholinesterase's *Ee*AChE, *Hu*AChE and *Hu*BChE which was in accordance with the developed 3D-QSAR model.

Compounds **8-10** were found to bind reversibly and non-competitively to AChE and showed moderate level of protection of *Hu*AChE against the irreversible inhibition by nerve agents tabun, soman and VX, although at higher concentrations in respect to their IC_{50} values. Compounds showed different levels of protection in relation to different nerve agents tested with compound **10** having the best protection against tabun irreversible inhibition, while compounds **8** and **9** were far superior against VX irreversible inhibition, comparing to compound **10**, which, although being the most potent subnanomolar inhibitor, provided only a marginal protection. Based on the results obtained and current available literature data, it still remains an open question whether this level of protection observed *in vitro* would be significant also *in vivo*. However, taking into consideration that there are some reversible inhibitors which actually increase the rates of AChE phosphylation [41] and that even moderately effective AChE reversible inhibitors such as ranitidine [16] improve survival of the experimental animals, it may be concluded that compounds **8–10** might be a promising leads in development of more effective protective agents.

The 100 ns long MD simulation initiated to study the compound **10** proposed binding mode in the AChE revealed that compound's moieties engage in several stable hydrophobic interactions, and both main moieties provide stable interactions with the targeted AS and PAS sites. Furthermore, a hydrogen bond between the amino group next to the

tacrine moiety and Met85 side chain oxygen and the ionic interaction between the protonated linker amino group and negatively charged Asp74 carboxylate side chainalso play a role in molecular recognition. The later ionic interaction provides one of the core contributions to the total interaction energy. The designed compounds thus represent promising leads for further development of more effective pre-treatment options against nerve agents.

Conflicts of interest

The authors declare that they have no conflict of interest.

Ethical standards

The manuscript does not contain clinical studies or patient data.

Acknowledgements

This work was supported by the Serbian Ministry of Education Science and Technological Development (grant OI172035), the Serbian Ministry of Defence, and by the German Ministry of Defence. AP was supported by the Ministry of Higher Education, Science and Technology of the Republic of Slovenia through Grant P1-0012. The authors are grateful to G. Duman for expert technical assistance and prof. Gerhard Wolber for providing us access to dynophore calculations at the Freie Universität Berlin, Germany.

Transparency document

Transparency document related to this article can be found online at https://doi.org/10.1016/j.cbi.2019.06.027.

Appendix A. Supplementary data

Supplementary data to this article can be found online at https://doi.org/10.1016/j.cbi.2019.06.027.

References

[1] A. Levy, G. Cohen, E. Gilat, R. Duvdevani, N. Allon, S. Shapira, S. Dachir, E. Grauer, Y. Meshulam, I. Rabinovitz, Therapeutic versus prophylactic treatment strategies against nerve-agent induced brain injuries, Proc. Med. Def. Biosci. Rev. US-AMRMC, Balt. (2000) 280–290.
[2] P. Eyer, D. Kiderlen, V. Meischner, L. Szinicz, H. Thiermann, F. Worek, The current status of oximes in the treatment of OP poisoning—comparing two regimes. Rome: european Association of Poisons Centres and Clinical Toxicologists, J. Toxicol. Clin. Toxicol. 41 (2003) 441–443 May 2003. Abstract.
[3] F. Worek, H. Thiermann, L. Szinicz, P. Eyer, Kinetic analysis of interactions between human acetylcholinesterase, structurally different organophosphorus compounds and oximes, Biochem. Pharmacol. 68 (2004) 2237–2248.
[4] Y. Ashani, A.K. Bhattacharjee, H. Leader, A. Saxena, B.P. Doctor, Inhibition of cholinesterases with cationic phosphonyl oximes highlights distinctive properties of the charged pyridine groups of quaternary oxime reactivators, Biochem. Pharmacol. 66 (2003) 191–202.
[5] D. Kiderlen, P. Eyer, F. Worek, Formation and disposition of diethylphosphoryl-obidoxime, a potent anticholinesterase that is hydrolyzed by human paraoxonase (PON1), Biochem. Pharmacol. 69 (2005) 1853–1867.
[6] W.K. Berry, D.R. Davies, The use of carbamates and atropine in the protection of animals against poisoning by 1, 2, 2-trimethylpropyl methylphosphonofluoridate, Biochem. Pharmacol. 19 (1970) 927–934.
[7] P. Dirnhuber, M.C. French, D.M. Green, L. Leadbeater, J.A. Stratton, The protection of primates against soman poisoning by pretreatment with pyridostigmine, J. Pharm. Pharmacol. 31 (1979) 295–299.
[8] L.W. Harris, D.L. Stitcher, W.C. Heyl, The effects of pretreatments with carbamates, atropine and mecamylamine on survival and on soman-induced alterations in rat and rabbit brain acetylcholine, Life Sci. 26 (1980) 1885–1891.
[9] L. Leadbeater, R.H. Inns, J.M. Rylands, Treatment of poisoning by soman, Fundam. Appl. Toxicol. 5 (1985) S225–S231.
[10] W.J. Lennox, L.W. Harris, D.R. Anderson, R.P. Solana, M.L. Murrow, J.V. Wade, Successful pretreatment/therapy of soman, sarin and VX intoxication, Drug Chem. Toxicol. 15 (1992) 271–283.
[11] Y. Meshulam, R. Davidovici, A. Wengier, A. Levy, Prophylactic transdermal treatment with physostigmine and scopolamine against soman intoxication in Guinea-pigs, J. Appl. Toxicol. 15 (1995) 263–266.
[12] Y. Meshulam, G. Cohen, S. Chapman, D. Alkalai, A. Levy, Prophylaxis against organophosphate poisoning by sustained release of scopolamine and physostigmine, J. Appl. Toxicol. An Int. J. 21 (2001) S75–S78.
[13] W.-S. Kim, Y. Cho, J.-C. Kim, Z.-Z. Huang, S.-H. Park, E.-K. Choi, S. Shin, S.-Y. Nam, J.-K. Kang, S.-Y. Hwang, Protection by a transdermal patch containing physostigmine and procyclidine of soman poisoning in dogs, Eur. J. Pharmacol. 525 (2005) 135–142.
[14] E.X. Albuquerque, E.F.R. Pereira, Y. Aracava, W.P. Fawcett, M. Oliveira, W.R. Randall, T.A. Hamilton, R.K. Kan, J.A. Romano, M. Adler, Effective countermeasure against poisoning by organophosphorus insecticides and nerve agents, Proc. Natl. Acad. Sci. U.S.A. 103 (2006) 13220–13225.
[15] G. Lallement, V. Baille, D. Baubichon, P. Carpentier, J.-M. Collombet, P. Filliat, A. Foquin, E. Four, C. Masqueliez, G. Testylier, Review of the value of huperzine as pretreatment of organophosphate poisoning, Neurotoxicology 23 (2002) 1–5.
[16] G.A. Petroianu, S.M. Nurulain, M. Shafiullah, M.Y. Hasan, K. Kuča, D.E. Lorke, Usefulness of administration of non-organophosphate cholinesterase inhibitors before acute exposure to organophosphates: assessment using paraoxon, J. Appl. Toxicol. 33 (2013) 894–900.
[17] M.D. Vitorović-Todorović, I.N. Cvijetić, I.O. Juranić, B.J. Drakulić, The 3D-QSAR study of 110 diverse, dual binding, acetylcholinesterase inhibitors based on alignment independent descriptors (GRIND-2). The effects of conformation on predictive power and interpretability of the models, J. Mol. Graph. Model. 38 (2012) 194–210.
[18] M.D. Vitorović-Todorović, I.O. Juranić, L.M. Mandić, B.J. Drakulić, 4-Aryl-4-oxo-N-phenyl-2-aminylbutyramides as acetyl-and butyrylcholinesterase inhibitors. Preparation, anticholinesterase activity, docking study, and 3D structure–activity relationship based on molecular interaction fields, Bioorg. Med. Chem. 18 (2010) 1181–1193.
[19] M.D. Vitorović-Todorović, C. Koukoulitsa, I.O. Juranić, L.M. Mandić, B.J. Drakulić, Structural modifications of 4-aryl-4-oxo-2-aminylbutanamides and their acetyl-and butyrylcholinesterase inhibitory activity. Investigation of AChE–ligand interactions by docking calculations and molecular dynamics simulations, Eur. J. Med. Chem. 81 (2014) 158–175.
[20] G.L. Ellman, K.D. Courtney, V. Andres Jr., R.M. Featherstone, A new and rapid colorimetric determination of acetylcholinesterase activity, Biochem. Pharmacol. 7 (1961) 88–95.
[21] F. Worek, T. Wille, M. Koller, H. Thiermann, Reactivation kinetics of a series of related bispyridinium oximes with organophosphate-inhibited human acetylcholinesterase—structure–activity relationships, Biochem. Pharmacol. 83 (2012) 1700–1706.
[22] F. Worek, U. Mast, D. Kiderlen, C. Diepold, P. Eyer, Improved determination of acetylcholinesterase activity in human whole blood, Clin. Chim. Acta 288 (1999) 73–90.
[23] Å. Forsberg, G. Puu, Kinetics for the inhibition of acetylcholinesterase from the electric eel by some organophosphates and carbamates, Eur. J. Biochem. 140 (1984) 153–156.
[24] N. Aurbek, H. Thiermann, L. Szinicz, P. Eyer, F. Worek, Analysis of inhibition, reactivation and aging kinetics of highly toxic organophosphorus compounds with human and pig acetylcholinesterase, Toxicology 224 (2006) 91–99.
[25] J. Cheung, M.J. Rudolph, F. Burshteyn, M.S. Cassidy, E.N. Gary, J. Love, M.C. Franklin, J.J. Height, Structures of human acetylcholinesterase in complex with pharmacologically important ligands, J. Med. Chem. 55 (2012) 10282–10286.
[26] A. Waterhouse, M. Bertoni, S. Bienert, G. Studer, G. Tauriello, R. Gumienny, F.T. Heer, T.A.P. de Beer, C. Rempfer, L. Bordoli, R. Lepore, T. Schwede, SWISS-MODEL: homology modelling of protein structures and complexes, Nucleic Acids Res. 46 (2018) W296–W303.
[27] T.A. Halgren, MMFF VI. MMFF94s option for energy minimization studies, J. Comput. Chem. 20 (1999) 720–729.
[28] J.J.P. Stewart, Optimization of parameters for semiempirical methods VI: more modifications to the NDDO approximations and re-optimization of parameters, J. Mol. Model. 19 (2013) 1–32.
[29] T.J. Dolinsky, P. Czodrowski, H. Li, J.E. Nielsen, J.H. Jensen, G. Klebe, N.A. Baker, PDB2PQR: expanding and upgrading automated preparation of biomolecular structures for molecular simulations, Nucleic Acids Res. 35 (2007) W522–W525.
[30] O. Trott, A.J. Olson, AutoDock Vina, Improving the speed and accuracy of docking with a new scoring function, efficient optimization, and multithreading, J. Comput. Chem. 31 (2010) 455–461.
[31] O. Korb, T. Stützle, T.E. Exner, PLANTS: application of ant colony optimization to structure-based drug design, in: M. Dorigo, L.M. Gambardella, M. Birattari, A. Martinoli, R. Poli, T. Stützle (Eds.), Ant Colony Optim. Swarm Intell. Springer Berlin Heidelberg, Berlin, Heidelberg, 2006, pp. 247–258.
[32] A. Pedretti, L. Villa, G. Vistoli, VEGA – an open platform to develop chemo-bioinformatics applications, using plug-in architecture and script programming, J. Comput. Aided Mol. Des. 18 (2004) 167–173.
[33] S. Jo, T. Kim, V.G. Iyer, W. Im, CHARMM-GUI: a web-based graphical user interface for CHARMM, J. Comput. Chem. 29 (2008) 1859–1865.
[34] J. Huang, S. Rauscher, G. Nawrocki, T. Ran, M. Feig, B.L. de Groot, H. Grubmüller, A.D. MacKerell Jr., CHARMM36m: an improved force field for folded and intrinsically disordered proteins, Nat. Methods 14 (2016) 71–73.
[35] K. Vanommeslaeghe, E. Hatcher, C. Acharya, S. Kundu, S. Zhong, J. Shim, E. Darian, O. Guvench, P. Lopes, I. Vorobyov, A.D. Mackerell, CHARMM general force field: a force field for drug-like molecules compatible with the CHARMM all-atom additive biological force fields, J. Comput. Chem. 31 (2009) 671–690.
[36] J.C. Phillips, R. Braun, W. Wang, J. Gumbart, E. Tajkhorshid, E. Villa, C. Chipot, R.D. Skeel, L. Kalé, K. Schulten, Scalable molecular dynamics with NAMD, J. Comput. Chem. 26 (2005) 1781–1802.
[37] W. Humphrey, A. Dalke, K. Schulten, VMD: visual molecular dynamics, J. Mol.

Graph. 14 (1996) 33–38.
[38] M. Bermudez, C. Rakers, G. Wolber, Structural characteristics of the allosteric binding site represent a key to subtype selective modulators of muscarinic acetylcholine receptors, Mol. Inform. 34 (2015) 526–530.
[39] A. Bock, M. Bermudez, F. Krebs, C. Matera, B. Chirinda, D. Sydow, C. Dallanoce, U. Holzgrabe, M. De Amici, M.J. Lohse, G. Wolber, K. Mohr, Ligand binding ensembles determine graded agonist efficacies at a G protein-coupled receptor, J. Biol. Chem. 291 (2016) 16375–16389.
[40] G. Wolber, T. Langer, LigandScout: 3-D pharmacophores derived from protein-bound ligands and their use as virtual screening filters, J. Chem. Inf. Model. 45 (2005) 160–169.
[41] Z. Radić, P. Taylor, The influence of peripheral site ligands on the reaction of symmetric and chiral organophosphates with wildtype and mutant acetylcholinesterases, Chem. Biol. Interact. 119 (1999) 111–117.
[42] G. Petroianu, U. Beha, C. Roth, W. Bergler, R. Rüfer, L-lactate protects in vitro acetylcholinesterase (AChE) from inhibition by paraoxon (E 600), J. Appl. Toxicol. An Int. J. 20 (2000) 249–257.
[43] G. Petroianu, K. Arafat, M. Kosanovic, A. Saleh, V. Camasamudram, M.Y. Hasan, In vitro protection of red blood cell acetylcholinesterase by metoclopramide from inhibition by organophosphates (paraoxon and mipafox), J. Appl. Toxicol. An Int. J. 23 (2003) 447–451.
[44] G.A. Petroianu, K. Arafat, A. Schmitt, M.Y. Hasan, Weak inhibitors protect cholinesterases from strong inhibitors (paraoxon): in vitro effect of ranitidine, J. Appl. Toxicol. An Int. J. 25 (2005) 60–67.
[45] G.A. Petroianu, M.Y. Hasan, S.M. Nurulain, M. Shafiullah, R. Sheen, N. Nagelkerke, Ranitidine in acute high-dose organophosphate exposure in rats: effect of the time-point of administration and comparison with pyridostigmine, Basic Clin. Pharmacol. Toxicol. 99 (2006) 312–316.
[46] B. Nizami, D. Sydow, G. Wolber, B. Honarparvar, Molecular insight on the binding of NNRTI to K103N mutated HIV-1 RT: molecular dynamics simulations and dynamic pharmacophore analysis, Mol. Biosyst. 12 (2016) 3385–3395.
[47] J. Mortier, C. Rakers, M. Bermudez, M.S. Murgueitio, S. Riniker, G. Wolber, The impact of molecular dynamics on drug design: applications for the characterization of ligand-macromolecule complexes, Drug Discov. Today 20 (2015) 686–702.